RESEARCH ARTICLE
SOLID EARTH: GEODYNAMICS

*Earth and Planetary Physics*
*10*: 22–29, 2026
doi: 10.26464/epp2026010

# Integrated $N_2$–Ar measurements of trace extraterrestrial samples

**Fei Su[1*], XuHang Zhang[1,2], ChuanTong Zhang[3], YouJuan Li[1], ZiHeng Liu[1], JianNan Li[1], HeJiu Hui[4], and HuaiYu He[1,2]**

[1]Key Laboratory of Planetary Science and Frontier Technology, Institute of Geology and Geophysics, Chinese Academy of Sciences, Beijing 100029, China;

[2]College of Earth and Planetary Sciences, University of Chinese Academy of Sciences, Beijing 100029, China;

[3]Institution of Meteorites and Planetary Materials Research, Guilin University of Technology, Guilin 541006, China;

[4]State Key Laboratory for Mineral Deposits Research and Lunar and Planetary Science Institute, School of the Earth Sciences and Engineering, Nanjing University, Nanjing 210093, China

**Key Points:**

- We developed a measurement system for the integrated analysis of $N_2$ and Ar isotopes from submilligram samples.
- The newly established measurement system is characterized by an exceptionally low background (total N blank ≤0.4 ng), ensuring reliable determination of $N_2$ isotopes.
- The integrated $N_2$–Ar analysis method holds promise for investigating a variety of extraterrestrial materials, including lunar samples and future asteroid-return missions.

**Citation:** Su, F., Zhang, X. H., Zhang, C. T., Li, Y. J., Liu, Z. H., Li, J. N., Hui, H. J., and He, H. Y. (2026). Integrated $N_2$–Ar measurements of trace extraterrestrial samples. *Earth Planet. Phys.*, *10*(1), 22–29. http://doi.org/10.26464/epp2026010

**Abstract:** As one of the major volatile components in extraterrestrial materials, nitrogen ($N_2$) isotopes serve not only as tracers for the formation and evolution of the solar system, but also play a critical role in assessing planetary habitability and the search for extraterrestrial life. The integrated measurement of $N_2$ and argon (Ar) isotopes by using noble gas mass spectrometry represents a state-of-the-art technique for such investigations. To support the growing demands of planetary science research in China, we have developed a high-efficiency, high-precision method for the integrated analysis of $N_2$ and Ar isotopes. This was achieved by enhancing gas extraction and purification systems and integrating them with a static noble gas mass spectrometer. This method enables integrated $N_2$–Ar isotope measurements on submilligram samples, significantly improving sample utilization and reducing the impact of sample heterogeneity on volatile analysis. The system integrates $CO_2$ laser heating, a modular two-stage Zr–Al getter pump, and a CuO furnace-based purification process, effectively reducing background levels ($N_2$ blank as low as $0.35 \times 10^{-6}$ cubic centimeters at standard temperature and pressure [ccSTP]). Analytical precision is ensured through calibration with atmospheric air and CO corrections. To validate the reliability of the method, we performed $N_2$–Ar isotope analyses on the Allende carbonaceous chondrite, one of the most extensively studied meteorites internationally. The measured $N_2$ concentrations range from 19.2 to 29.8 ppm, with $\delta^{15}N$ values between −44.8‰ and −33.0‰. Concentrations of $^{40}Ar$, $^{36}Ar$, and $^{38}Ar$ are (12.5–21.1) × $10^{-6}$ ccSTP/g, (90.9–150.3) × $10^{-9}$ ccSTP/g, and (19.2–30.7) × $10^{-9}$ ccSTP/g, respectively. These values correspond to cosmic-ray exposure ages of 4.5–5.7 Ma, consistent with previous reports. Step-heating experiments further reveal distinct release patterns of N and Ar isotopes, as well as their associations with specific mineral phases in the meteorite. In summary, the combined $N_2$–Ar isotopic system offers significant advantages for tracing volatile sources in extraterrestrial materials and will provide essential analytical support for upcoming Chinese planetary missions, such as Tianwen-2.

**Keywords:** integrated $N_2$–Ar measurement; noble gas mass spectrometer; extraterrestrial samples

## 1. Introduction

As the sixth most abundant element in the solar system (Lodders, 2003), nitrogen

$$\left\{\delta^{15}N = \left[\left(\frac{^{15}N}{^{14}N}\right)_{sample} \Big/ \left(\frac{^{15}N}{^{14}N}\right)_{air} - 1\right] \times 1000\right\}$$

displays a remarkably variable isotopic composition, ranging from −483‰ to +4500‰ among solar system bodies and their constituent materials. $\delta^{15}N$ is in ‰. This pronounced isotopic heterogeneity makes nitrogen a valuable tracer for investigating the origin of volatiles as well as the processes of planetary formation and evolution (Hashizume et al., 2000; Füri and Marty, 2015). Asteroid exploration has emerged as a primary objective in the next phase of China's deep space missions (Liu B et al., 2023; Jiao YF et al., 2024; Wei SJ et al., 2024). Elucidating the origin of asteroid materials and their genetic relationships to different meteorite groups represents a central scientific challenge in modern planetary geochemistry (Lin YT et al., 2020). Integrated $N_2$ and Ar isotope measurements in asteroid samples offer significant poten-

Correspondence to: F. Su, sufei@mail.iggcas.ac.cn
Received 30 JUN 2025; Accepted 18 SEP 2025.
First Published online 31 OCT 2025.

tial for tracing their source reservoirs and identifying links to corresponding meteorite types (Broadley et al., 2023). For example, noble gas and nitrogen isotope data from the Hayabusa2-returned samples exhibit isotopic signatures similar to those of CI chondrites, suggesting a close genetic relationship between asteroid Ryugu and CI-type meteorites (Okazaki et al., 2022). China's Tianwen-2 mission will return samples from the near-Earth asteroid 2016 $HO_3$, and integrated $N_2$–Ar isotopic analyses of these samples are expected to place important constraints on the origin and evolutionary history of volatiles on this small body. In addition, the N and Ar isotopes in lunar samples can provide constraints on the transport of volatiles within the solar system (Zhang H et al., 2023; Cao JB et al., 2024).

Conventional N isotope analyses have typically relied on dynamic mode measurements using isotope ratio mass spectrometry, requiring sample quantities of approximately ~100 mg (Chang et al., 1974; Thiemens and Clayton, 1981). This requirement makes the method unsuitable for analyzing rare extraterrestrial materials that are available only in submilligram quantities. Recent advances in static noble gas mass spectrometry have enabled high-precision measurements of trace amounts of $N_2$ (Humbert et al., 2000; Barry et al., 2012). Wright et al. (1988) demonstrated high-precision $N_2$ isotope ratio measurements at the nanomole level by using noble gas mass spectrometry. Humbert et al. (2000) further improved the technique by utilizing $CO_2$ laser heating and a high-sensitivity, high-resolution mass spectrometer in static mode, enabling accurate quantification of $N_2$ at the picomole scale. The system exhibited an exceptionally low blank level of ~2 pmol of $N_2$ (equivalent to ~60 pg of N), allowing for routine analysis of milligram-sized samples, such as mantle-derived minerals, meteorite constituents, and lunar soil particles. Building on this progress, Barry et al. (2012) used a modified VG-5440 noble gas mass spectrometer to perform multicollector measurements of all three nitrogen isotopes from <0.5 nmol of $N_2$ ($<10^{-3}$ ccSTP), further demonstrating the suitability of noble gas systems for low-level nitrogen isotopic analysis. These developments have established noble gas mass spectrometry as a leading technique for investigating volatile components in extraterrestrial materials. However, the application of this technique remains largely absent in China.

In this study, we address key technical challenges in integrated N–Ar isotope analysis—the efficient separation and purification of reactive and noble gases—by modifying an existing noble gas mass spectrometry system. This modification enables integrated measurements of N and Ar isotopes from submilligram samples. The method was validated using the Allende carbonaceous chondrite, confirming the capability of the system to accurately determine elemental abundance and isotopic composition. This successful development offers a novel and robust analytical platform for future investigations of volatile components in extraterrestrial materials in China.

## 2. Analytical Method

### 2.1 Gas Extraction and Purification System

Figure 1 shows the integrated $N_2$–Ar isotope analytical system developed in this study, which consists of a gas extraction unit

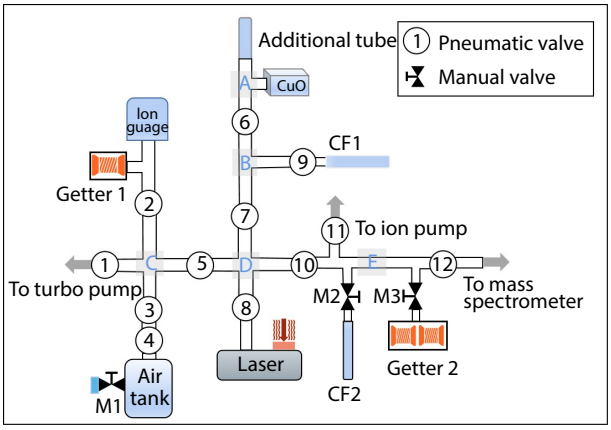


**Figure 1**. Schematic diagram of the extraction and purification piping of the integrated $N_2$–Ar measurement system.

and an ultra-high vacuum (UHV) purification line. Gas extraction is performed using $CO_2$ laser heating (wavelength: 10.6 μm; maximum power: 50 W). The sample chamber is made of 316L stainless steel and fitted with a chemical vapor deposition diamond window, which ensures high $CO_2$ laser transmittance, maintains UHV conditions, and minimizes background gas levels. The sample holder, which directly contacts the samples, is made of oxygen-free copper and can accommodate up to 20 individual samples, significantly increasing analytical throughput. All critical sealing interfaces use metal knife-edge flanges paired with oxygen-free copper gaskets, providing fully metallic, leak-tight seals essential for maintaining system integrity under UHV conditions.

The gas purification system adopts a modular design comprising two-stage Zr–Al getter pumps (SAES GP50), a CuO oxidation furnace, and a dual cold-trap configuration:

(1) The first-stage Zr–Al getter pump (Getter 1) minimizes $N_2$ background during the initial phase of analysis and is then isolated from the line during sample measurements via manual valve V2.

(2) The CuO oxidation furnace, equipped with a K-type thermocouple (maximum operating temperature: 1200 ± 5 °C), catalyzes the conversion hydrocarbons into $CO_2$ and $H_2O$.

(3) The quartz cold trap CF1, held at liquid nitrogen temperature (77 K), selectively adsorbs high-boiling-point species (e.g., $CO_2$ and $H_2O$) while allowing $N_2$ to pass through unimpeded.

(4) The second-stage Zr–Al getter pump (Getter 2), combined with an activated charcoal cold trap (CF2), facilitates low-temperature purification of Ar.

(5) A 5-liter standard gas tank is manually filled by drawing 3.75 $cm^3$ of atmospheric air via valve M1. A calibrated 0.1 $cm^3$ mini-volume, located upstream of the tank, enables precise aliquoting of isotopic calibration. With the exception of the CuO furnace and the CF1 cold trap, all components are made of electropolished 316L stainless steel. The internal volumes of each module were precisely determined using 99.99% pure He as a tracer gas, resulting in a measurement uncertainty below 1%. The system features volume of laser chamber of 100.2 cc, with the remaining parts A,

B, C, D, and E having volumes of 160.3 cc, 21.3 cc, 69.5 cc, 25.1 cc, and 127.0 cc, respectively.

### 2.2 Sample Analysis Protocol

Prepared samples were placed into the laser sample holder (Figure 1, Laser) and integrated with the UHV system. The vacuum line was evacuated and baked at 120 °C for ~48 hours to remove adsorbed atmospheric gases from the sample surfaces. Given that solar wind components are typically implanted only to depths of tens of nanometers, heating at this temperature does not alter their release characteristics. This has been confirmed by rare gas isotope analyses of lunar soil: samples baked at 120 °C still exhibited clear solar wind-derived rare gas signals, especially He isotopes, which retain typical solar wind signatures in the initial release stage (Zhang XH et al., 2024). If heating had affected these components, the He isotope ratios would have shown significant changes, yet no such variations were observed.

Gas extraction was performed using a $CO_2$ laser, via either total fusion or stepwise heating. In the total fusion mode, the sample is fully melted under ~90% of the laser's maximum output power to release all trapped gases. In the stepwise heating mode, the laser output power is carefully modulated to incrementally heat the sample, enabling gas release at distinct temperature intervals. This approach allows for the characterization of gas release profiles associated with specific mineral phases or trapping sites within the sample.

Gases released from the laser-heated sample diffused freely into four designated volumes: regions A, B, C, and D. Gas in region A was designated for the measuring of $N_2$ abundance and its isotopic composition. To increase the relative proportion of $N_2$, an additional tube was added to expand region A, raising its volume to ~43% of the total. The remaining gas, distributed across regions B, C, and D—including the laser sample chamber—was reserved for Ar isotope analysis, comprising ~57% of the total volume. Gas from regions B to D was then directed into region E for purification by a Zr–Al getter pump. The purified gas was trapped in CF2, a liquid nitrogen-cooled cold trap (77 K), where Ar was selectively adsorbed. After adsorption, residual gases—primarily He—were evacuated using an ion/molecular pump. The adsorbed Ar in CF2 was released by heating, repurified using the Zr–Al getter pump, and introduced into the mass spectrometer for isotopic analysis.

The gas designated for $N_2$ analysis in region A is first oxidized by $O_2$ released from a CuO furnace operated at 850 °C. This step primarily converts carbon-bearing species (e.g., CO, $C_xH_y$) into $CO_2$ and $H_2O$. Additionally, residual hydrogen- and sulfur-bearing compounds are oxidized to $H_2O$ and $SO_2$, respectively.

Excess $O_2$ not consumed during oxidation is subsequently removed through sequential absorption in the CuO furnace held at 600 °C and 450 °C. The gas mixture in region A then diffuses into region B, where condensable species produced during the oxidation process are cryogenically trapped in CF1, a cold trap at liquid nitrogen temperature. Finally, the purified gas is introduced into the mass spectrometer to determine the $N_2$ abundance and isotopic composition.

### 2.3 Measurement

Measurements of $N_2$ and Ar isotopes were performed using a Helix SFT noble gas mass spectrometer operating in peak-jumping mode. In the Ar isotopic analysis, $^{40}Ar$ was measured using a Faraday cup, whereas $^{38}Ar$ and $^{36}Ar$ were detected with an electron multiplier. Each acquisition comprised 11 measurement cycles. In the $N_2$ isotope analysis, masses 28 (primarily $^{14}N^{14}N$) and 29 (primarily $^{14}N^{15}N$) were measured using the Faraday cup, whereas mass 30 (predominantly $^{15}N^{15}N$) was detected with the electron multiplier.

To prevent premature filament failure resulting from excessive trap current, the trap current was deliberately reduced during integrated $N_2$–Ar measurements. Although this adjustment reduced sensitivity, the data quality remained unaffected because of the relatively high concentrations of N and Ar in the extraterrestrial samples. During the $N_2$ analysis, the trap current was set to 50 μA, resulting in a sensitivity of approximately $2.90 \times 10^{-11}$ ccSTP/fA. For the Ar analysis, the trap current was set to 150 μA, with a corresponding sensitivity of ~$5.05 \times 10^{-12}$ ccSTP/fA. Each analysis run included 11 cycles. Nitrogen isotopic ratios were determined by linearly extrapolating ion signals to time zero, corresponding to the sample gas entry point into the mass spectrometer.

Data correction procedures included baseline subtraction, interference correction for CO species, and normalization to an atmospheric air standard. Background measurements were routinely conducted between analyses, typically after every one to two sample or standard runs, to monitor and correct for instrumental drift and residual gas contributions.

### 2.4 Data Correction

#### *2.4.1 Standard air*

To ensure the analytical stability of the mass spectrometric system during the course of the experiments, standard gas measurements were periodically performed. These tests involved quantitative extraction of gas from a 5-liter standard air reservoir maintained at an initial pressure of approximately 0.57 torr. For each test, the extracted gas volume was precisely adjusted to 0.1 $cm^3$, producing nitrogen quantities in the range of ~$1.2 \times 10^{-6}$ to $1.2 \times 10^{-5}$ ccSTP, appropriate for matching the signal intensities of typical sample analyses.

A calibration curve was constructed by aligning the ion signal intensity of the standard gas with that of the samples, thereby correlating the measured $^{15}N/^{14}N$ isotopic ratio in standard air to the signal magnitude (Figure 2). This calibration procedure yielded an analytical precision better than 2‰ for the $^{15}N/^{14}N$ ratio, demonstrating the reliability of the system under the selected analytical conditions. It is important to note that this calibration curve is applicable only to the specific measurement session reported here. For different sets of samples or experimental runs, the calibration must be repeated to account for possible variations in system behavior, such as changes in detector gain or ion source conditions.

In contrast, no significant linear dependence was observed

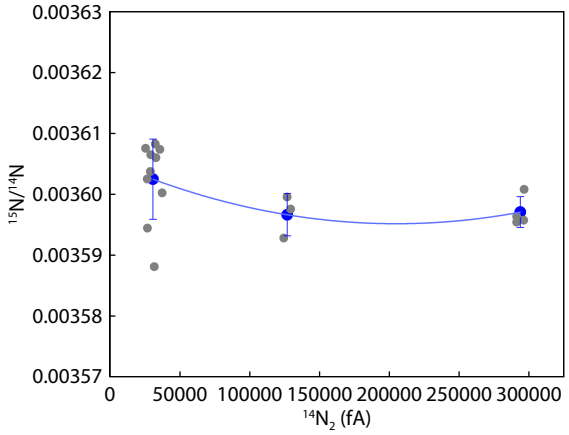


**Figure 2**. Calibration curve of nitrogen isotopes in standard air at different signal intensities. The gray data points represent the measured values of standard air. The blue data points indicate the average of multiple measurements with the same signal intensity (i.e., the gray data points), and the error bars represent one standard deviation (1 SD).

between the $^{40}Ar/^{36}Ar$ or $^{38}Ar/^{36}Ar$ ratios and the signal intensity of $^{40}Ar$. This result indicates that, within the range of signal intensities encountered, Ar isotopic measurements were not substantially affected by signal amplitude-related fractionation. As a result, Ar isotopic data were corrected by referencing the measured $^{40}Ar/^{36}Ar$ and $^{38}Ar/^{36}Ar$ ratios of each sample to the average values obtained from the full experimental dataset, which were $310.6 \pm 4.3$ and $0.191 \pm 0.002$, respectively. These values were used in comparison with the theoretical atmospheric ratios to perform internal normalization and correct for any instrumental drift or background interference. This approach ensured consistent Ar isotope data quality across all analyzed samples.

*2.4.2 Background correction*

Background correction is especially important for samples with low $N_2$ content. A full-procedure system blank analysis was conducted prior to each sample or standard air measurement. Throughout the experimental campaign, the $N_2$ background level of the system remained stable, showing a negligible difference between cold and hot blank conditions. The average background level was $0.35 \pm 0.05 \times 10^{-6}$ ccSTP ($1\sigma$), equivalent to ~0.4 ng of $N_2$. This background level is significantly lower than those reported by leading international laboratories for $N_2$ isotope analysis ($4.2–14.6 \times 10^{-6}$ ccSTP; Barry et al., 2012). The background contribution to the total $N_2$ in the samples was less than 10%.

A nitrogen isotope background correction was applied using the following equation (Barry et al., 2012):

$$\delta^{15}N_C = \frac{\delta^{15}N_S - \left[\delta^{15}N_B \times \frac{[N_2]_B}{[N_2]_S}\right]}{1 - \frac{[N_2]_B}{[N_2]_S}}.$$

In this equation, C, B, and S represent the corrected value, system background, and measured value of the sample, respectively.

The average system background for $^{40}Ar$ was ~$1.6 \pm 0.2 \times 10^{-9}$ ccSTP ($1\sigma$). The background correction was typically performed by subtracting the background value from the measured signal.

*2.4.3 Interference CO correction*

The extracted gas mixture contains carbon monoxide (CO) and diverse hydrocarbons. Although oxidation within the CuO purification furnace converts these species predominantly to $CO_2$ and $H_2O$, their complete elimination is not achieved. Consequently, residual CO interferes with the quantification of molecular nitrogen ($N_2$) during mass spectrometric analysis because of overlapping mass-to-charge $m/z$) ratios. Specifically, limited instrument resolution precludes the complete separation of signals at $m/z$ 28, 29, and 30, which represent composite intensities arising from $N_2$ and CO isotopologues. To resolve this interference, the correction protocol established by Barry et al. (2012) was applied. The signal contributions were defined by the following equations:

$$[M28] = [^{14}N^{14}N] + [^{12}C^{16}O], \quad (1)$$

$$[M29] = [^{14}N^{15}N] + [^{13}C^{16}O] + [^{12}C^{17}O], \quad (2)$$

$$[M30] = [^{15}N^{15}N] + [^{12}C^{18}O] + [^{13}C^{17}O], \quad (3)$$

where [MX] denotes the measured signal intensity at $^{*}m/z^{*}$ = X. Minor isotopologue contributions (enclosed in brackets) are negligible under standard analytical conditions and were excluded from subsequent calculations.

Assuming isotopic equilibrium, the relative abundance of $N_2$ isotopologues follows the statistical distribution:

$$[^{14}N^{14}N] : [^{14}N^{15}N] : [^{15}N^{15}N] = 1 : 2r : r^2, \quad (4)$$

where $r$ is the $^{15}N/^{14}N$ ratio. Further assuming that the isotopic ratios within CO ($^{13}C/^{12}C$, $^{18}O/^{16}O$, $^{17}O/^{16}O$) conform to natural terrestrial abundances, Equations (1 – 3) can be reformulated as

$$[M28] = [^{14}N^{14}N] + [^{12}C^{16}O], \quad (5)$$

$$[M29] = 2r \times [^{14}N^{14}N] + R^{13} \times [^{12}C^{16}O], \quad (6)$$

$$[M30] = r^2 \times [^{14}N^{14}N] + R^{18} \times [^{12}C^{16}O], \quad (7)$$

where $R^{13} = {}^{13}C/{}^{12}C$ and $R^{18} = {}^{18}O/{}^{16}O$ represent the natural abundance ratios. Solving this system of equations simultaneously yields the value of $r$ (the $^{15}N/^{14}N$ ratio). Additionally, the absolute concentrations of $^{14}N^{14}N$ and $^{12}C^{16}O$ can be derived, enabling quantification of the CO interference on the $N_2$ signal.

Given the significantly higher natural abundance of $^{14}N^{14}N$ and $^{14}N^{15}N$ compared with $^{15}N^{15}N$, the signal intensity at $m/z$ 30 ([M30]) serves as a robust indicator of the CO contribution. Application of this correction methodology revealed that CO contributed approximately 2% to the total signal intensity during sample analysis in this study.

## 3. $N_2$ and Ar Isotopes of the Meteorite Allende

### 3.1 Feasibility of the Method

To evaluate the reliability and performance of the newly developed integrated $N_2$–Ar measurement system and analytical protocol, we selected the Allende meteorite—a well-characterized CV3 carbonaceous chondrite from a witnessed fall—as the test

sample. The Allende meteorite primarily consists of coarse-grained, Mg-rich olivine and a fine-grained Fe-rich olivine matrix. It also contains abundant calcium–aluminum-rich inclusions (CAIs), which represent some of the earliest solid condensates formed during the cooling of the solar nebula. Despite having undergone moderate thermal metamorphism, Allende remains chemically heterogeneous, displaying distinct features of a nonequilibrated chondrite (Young and Russell, 1998; Cuvillier et al., 2015).

Schultz and Franke (2004) compiled a comprehensive dataset of Ar isotopic compositions in Allende, reporting whole-rock concentrations of $^{40}$Ar, $^{38}$Ar, and $^{36}$Ar ranging from (0.32–286.44) × $10^{-6}$, (3.6–53.5) × $10^{-9}$, and (6.5–176.0) × $10^{-9}$ ccSTP/g, respectively. The $^{36}$Ar/$^{38}$Ar ratios vary between 0.71 and 5.35. Nitrogen concentrations range from 18 to 70 ppm, with $\delta^{15}$N values spanning from –43‰ to –5‰ (Gibson et al., 1971; Kung and Clayton, 1978; Frick and Pepin, 1981). Despite extensive research on N and noble gas isotopes in Allende, no previous work has reported integrated N and Ar isotope analyses on the same sample aliquot. This study thus presents the first integrated $N_2$–Ar isotope measurements conducted on a single Allende specimen.

Four Allende samples were analyzed using the newly developed integrated $N_2$–Ar measurement system. Two samples underwent total melting, whereas the other two were subjected to step-heating extraction. The resulting $N_2$ and Ar isotopic data are summarized in Table 1 and Figure 3. The analytical uncertainties for isotopic concentrations are approximately 5%, whereas those for $\delta^{15}$N values are approximately 15%. Concentrations of $^{40}$Ar, $^{38}$Ar, and $^{36}$Ar are (12.5–21.1) × $10^{-6}$ ccSTP/g, (19.2–30.7) × $10^{-9}$ ccSTP/g, and (90.9–150.3) × $10^{-9}$ ccSTP/g, respectively. The $N_2$ concentrations range from 19.2 to 29.8 ppm, with $\delta^{15}$N values between –33.0‰ and –44.8‰. Cosmic ray exposure (CRE) ages were calculated using the relation $T_{38} = C_{38}/P_{38}$, where $C_{38}$ is the cosmogenic $^{38}$Ar content and $P_{38}$ is its production rate. The $P_{38}$ values were determined based on Eugster (1988), incorporating a corrected $(^{22}Ne/^{21}Ne)_c$ ratio of 1.11, as recommended by Wieler (2002). The calculated CRE ages range from 4.5 to 5.7 Ma, consistent within uncertainty with previously reported exposure ages of 5 ± 1 Ma (Das and Murty, 2009). The temperature-dependent behavior of N isotopes closely matches the classic pattern reported by Thiemens and Clayton (1981). At lower temperatures, $\delta^{15}$N values are influenced by atmospheric contamination and approach the atmospheric endmember. With increasing temperature, $\delta^{15}$N values decrease, indicating a shift toward the isotopic composition of the primordial solar nebula. At higher temperatures, $\delta^{15}$N values increase slightly, likely because of cosmogenic $^{15}$N, resulting in a characteristic V-shaped $\delta^{15}$N–temperature trend (Figure 4). The close agreement between the isotopic signatures and CRE ages obtained in this study and those reported previously strongly supports the accuracy and reliability of the newly developed N–Ar analytical method. Although the Allende meteorite had long been stored in an atmospheric environment, the N and Ar isotope results showed no interference from storage, further

**Table 1.** N–Ar isotopes of meteorite Allende.

| | Laser output power (%) | $^{40}$Ar (×$10^{-6}$ ccSTP/g) | $^{36}$Ar (×$10^{-9}$ ccSTP/g) | $^{38}$Ar (×$10^{-9}$ ccSTP/g) | $T_{38}$ (Ma) | $N_2$ (ppm) | $\delta^{15}$N (‰)[a] | $^{36}Ar_{tr}/N_2$ |
|---|---|---|---|---|---|---|---|---|
| Total fusion | | | | | | | | |
| Allende-T1, 0.622 mg | | 21.08 | 150.28 | 30.71 | 5.74 | 29.81 | –44.83 | 6.72E-06 |
| Allende-T2, 0.384 mg | | 16.04 | 103.09 | 21.55 | 5.03 | 19.21 | –33.02 | 7.13E-06 |
| Step heating | | | | | | | | |
| Allende-S1, 2.523 mg | 3 | 2.48 | 7.70 | 1.44 | | 1.68 | 4.01 | |
| | 4 | 3.92 | 2.49 | 0.72 | | 2.72 | 0.04 | |
| | 5 | 1.89 | 2.25 | 0.60 | | 3.97 | –32.54 | |
| | 6 | 1.12 | 2.46 | 0.79 | | 1.78 | –95.31 | |
| | 8 | 0.40 | 1.92 | 0.34 | | 0.46 | –98.48 | |
| | 90 | 4.87 | 81.25 | 16.47 | | 10.59 | –48.67 | |
| | Total | 14.67 | 98.07 | 20.36 | 4.48 | 21.20 | –40.23 | 6.15E-06 |
| Allende-S2, 3.189 mg | | | | | | | | |
| | 3 | 7.70 | 8.30 | 1.75 | | 2.33 | 3.04 | |
| | 4 | 2.49 | 4.23 | 0.88 | | 5.09 | –16.58 | |
| | 5 | 2.25 | 5.97 | 1.28 | | 3.07 | –70.14 | |
| | 10 | 2.46 | 40.50 | 8.61 | | 8.04 | –47.90 | |
| | 20 | 1.92 | 21.92 | 4.50 | | 2.93 | –34.36 | |
| | 90 | 81.25 | 10.01 | 2.14 | | 0.75 | –44.27 | |
| | Total | 98.07 | 90.94 | 19.15 | 4.76 | 22.21 | –36.56 | 5.43E-06 |

[a]No correction for cosmogenic N.

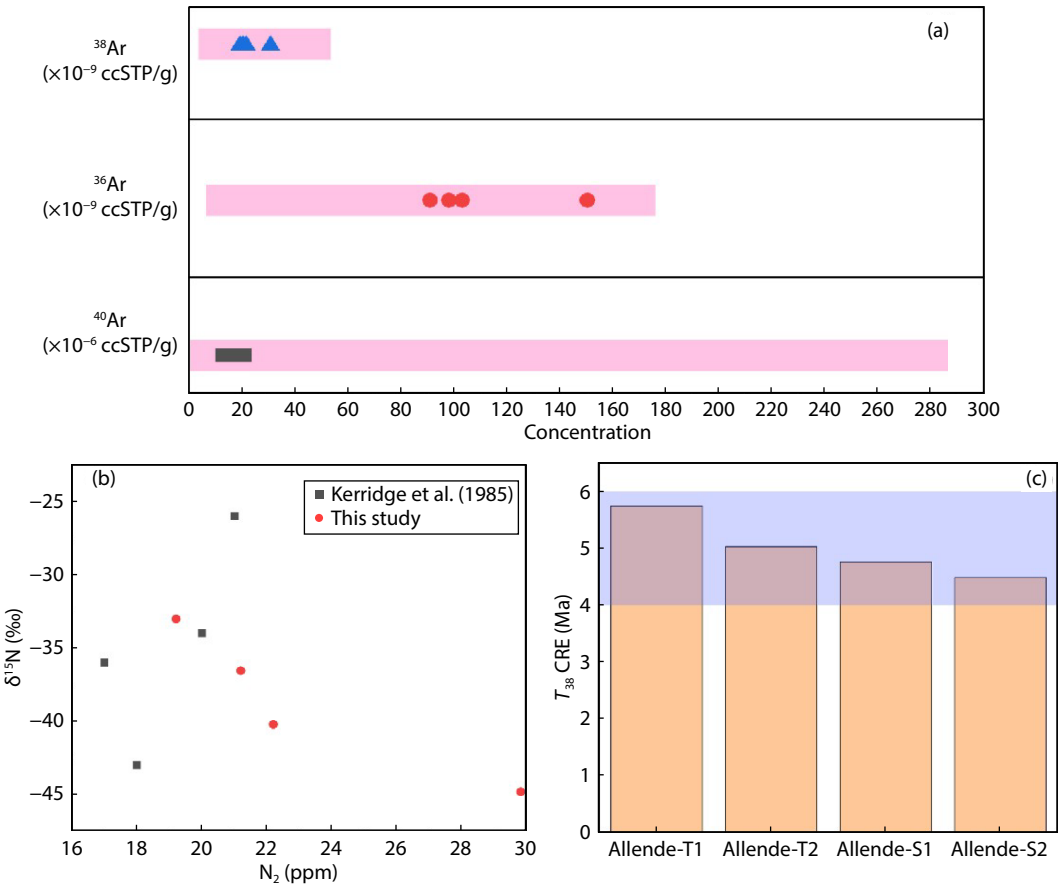


**Figure 3**. N and Ar isotopic signatures of the Allende meteorite. (a) Ar isotope results. The shaded areas are published ranges of Ar isotope content, with data from Schultz and Franke (2004). The data points are measurements from this study. (b) N isotope results. (c) $T_{38}$ CRE age distribution of the Allende meteorite in this study. The shaded area is the previously accepted CRE age of 5 ± 1 Ma for the Allende meteorite.

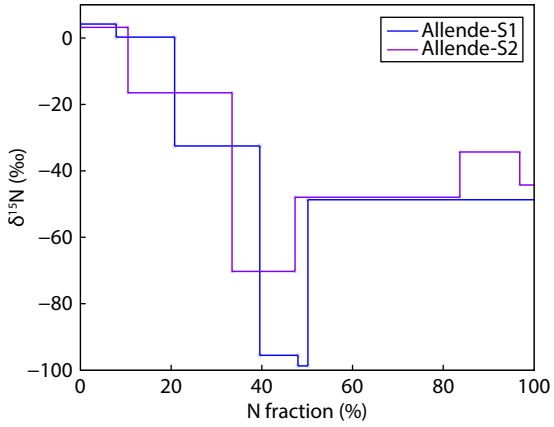


**Figure 4**. N isotope release characteristics of the Allende meteorite.

confirming the effectiveness of the experimental sample-handling procedures.

### 3.2 Release Character of N and Ar Isotopes

Step-heating experiments using a $CO_2$ laser were conducted by progressively increasing the output power to achieve controlled temperature increments. This technique provides high heating efficiency and low system background, making it the standard method for stepwise noble gas isotopic analyses in modern noble gas laboratories. Although infrared optical pyrometers can be utilized to monitor temperature, they often fail to accurately reflect the true heating temperature of the sample, complicating precise temperature determination. After each heating step, the released gases were analyzed for both N and Ar isotopic measurements, allowing characterization of their release behaviors. The amount of released gas is closely correlated with the magnitude of temperature increase. In practice, temperature steps are often adjusted according to the release profile of a specific isotope, such as $^{40}$Ar. However, gas release often occurs over discrete temperature intervals, resulting in step-specific concentrations (Figures 5a and 5c). For example, in sample S1, the final heating step released only 33% of the total $^{40}$Ar yet accounted for more than 80% of the total $^{36}$Ar and $^{38}$Ar and approximately 50% of the total $N_2$ (Figure 5a). This pattern likely reflects the combination of high-temperature cosmogenic gas components (typically released at elevated temperatures; Manuel et al., 1972) and the varying degassing temperatures of different mineral phases (Frick and Pepin, 1981).

In contrast, sample S2 exhibited a distinct degassing pattern, in which both N and Ar isotope releases followed a parallel rise-and-fall trend across temperature steps (Figure 5c). These intersample differences are further reflected in the Ar isotopic ratios. As shown in Figures 5b and 5d, both samples display similar $^{40}$Ar/$^{36}$Ar trends, which increase initially and then decrease with tempera-

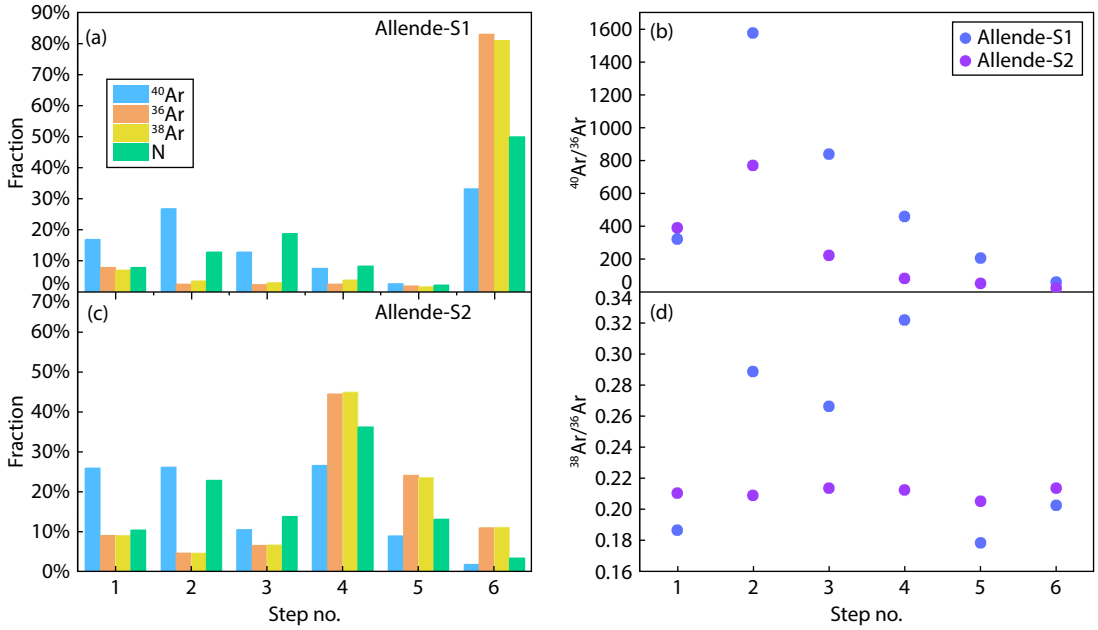


**Figure 5**. Character of Ar isotope release.

ture, reaching peak values of ~1753 for S1 and ~769 for S2. This behavior is interpreted as reflecting the release of radiogenic $^{40}$Ar concentrated in intermediate temperature fractions. Additionally, the $^{38}$Ar/$^{36}$Ar ratios are relatively stable in S2 (ranging from 0.2054 to 0.2105) but vary significantly in S1 (ranging from 0.1868 to 0.2889). These variations in isotopic ratios highlight the intrinsic heterogeneity of the Allende meteorite, potentially resulting from differences in mineralogical composition and the relative abundances of cosmogenic and neutron-capture products within the analyzed fragments (Manuel et al., 1972).

### 3.3 Potential Application of the Method to Lunar or Asteroid Samples

The system blank level is critical for reliable N isotope measurements in extraterrestrial materials. Apollo samples—including regolith, breccia, feldspar, and ilmenite—contain 3–407 ppm of N (Frick et al., 1988; Kerridge, 1993; Wieler et al, 1999; Assonov et al., 2002; Furi and Marty, 2015; Mortimer et al., 2015). Thus, a 1 mg aliquot is expected to contain at least ~3 ng of N. Our system contributes only 0.4 ng of N as blank—almost an order of magnitude below the minimum expected content of lunar samples. This ultralow background enables high-precision $\delta^{15}$N determinations in lunar materials.

The setup is equally suited to asteroid N isotope analyses. Early spectroscopy classified near-Earth asteroid 2016 $HO_3$ as an S-type or volatile-rich C-type (Reddy et al., 2017). Later orbital-dynamics modeling and spectral comparisons indicated a close compositional match to lunar farside ejecta from the Bruno crater. These data imply that 2016 $HO_3$ is lunar ejecta produced by an impact ~10 million years ago (Jiao JF et al., 2024). Consequently, the abundance and distribution of solar wind-implanted N in 2016 $HO_3$ should mirror those of lunar materials. The expected N concentration remains well above the 0.4 ng system blank. Even for C-type asteroids with high N contents—for example, Ryugu (~700 ppm; Okazaki et al., 2022)—a 0.4 ng blank adds negligible error to 1 mg analyses. Accordingly, the system satisfies the stringent requirements for high-confidence $\delta^{15}$N tracing in lunar and asteroid specimens.

## 4. Conclusions

In this study, we developed a novel analytical approach that enables the integrated measurement of $N_2$ and Ar isotopes in trace amounts of extraterrestrial materials. This was accomplished through the innovative design of a gas extraction and purification system, representing the first implementation of such a method in China. The system is characterized by an ultralow background level ($N_2$ blank as low as $0.35 \times 10^{-6}$ ccSTP, ~0.4 ng), high analytical precision ($\delta^{15}$N reproducibility better than 2‰, with elemental abundance uncertainties ≤5%), and minimal sample consumption (submilligram level). This integrated determination of $N_2$ and Ar isotopes in a single run significantly improves sample utilization efficiency and reduces the influence of sample heterogeneity on the interpretation of volatile components in extraterrestrial materials. The combined use of $N_2$ and Ar isotopes provides a powerful tool for tracing the origin and evolution of planetary volatiles. As China's Tianwen-2 asteroid sample return mission targeting asteroid 2016 $HO_3$ progresses, this analytical protocol will offer essential technical support for the volatile investigations of returned asteroid samples.

## Acknowledgments

This work was supported by the Bureau of Frontier Sciences and Basic Research, Chinese Academy of Sciences (Grant No. QYJ-2025-0103), the National Natural Science Foundation of China (Grant Nos. 42441834, 42241105, 42441825, and 42203048), and the Key Research Program of the Institute of Geology and Geophysics, Chinese Academy of Sciences (Grant No. IGGCAS-202401).

## References


Assonov, S. S., Franchi, I. A., Pillinger, C. T., Semenova, A. S., Shukolyukov, Y. A., Verchovsky, A. B., and Iassevitch, A. N. (2002). Nitrogen and argon release profiles in Luna 16 and Luna 24 regolith samples: The effects of regolith reworking. *Meteorit. Planet. Sci.*, *37*(1), 27–48. https://doi.org/10.1111/j.1945-5100.2002.tb00794.x

Barry, P. H., Hilton, D. R., Halldórsson, S. A., Hahm, D., and Marti, K. (2012). High precision nitrogen isotope measurements in oceanic basalts using a static triple collection noble gas mass spectrometer. *Geochem. Geophys. Geosyst.*, *13*, Q01019. https://doi.org/10.1029/2011GC003878

Broadley, M. W., Byrne, D. J., Füri, E., Zimmermann, L., Marty, B., Okazaki, R., Yada, T. Kitajima, F., Tachibana, S., … Uemura, R. (2023). The noble gas and nitrogen relationship between Ryugu and carbonaceous chondrites. *Geochim. Cosmochim. Acta*, *345*, 62–74. https://doi.org/10.1016/j.gca.2023.01.020

Cao, J. B., Wang, H. Z., Zhang, J., and Shi, Q. Q. (2024). Key questions of Earth wind–Moon interaction. *Space Sci. Technol.*, *4*, 0094. https://doi.org/10.34133/space.0094

Chang, S., Lawless, M., Romie, M., Kaplan, I. R., Petrowski, C., Sakai, H., and Smith, J. W. (1974). Carbon, nitrogen and sulfur in lunar fines 15012 and 15013: Abundances, distributions and isotopic compositions. *Geochim. Cosmochim. Acta*, *38*, 853–872. https://doi.org/10.1016/0016-7037(74)90060-X

Cuvillier, P., Leroux, H., Jacob, D., and Hirel, P. (2015). Fe-Mg interdiffusion profiles in rimmed forsterite grains in the Allende matrix: Time–temperature constraints for the parent body metamorphism. *Meteorit. Planet. Sci.*, *50*(9), 1529–1545. https://doi.org/10.1111/maps.12493

Das, J. P., and Murty, S. V. S. (2009). Cosmogenic and trapped noble gases in individual chondrules: Clues to chondrule formation. *Meteorit. Planet. Sci.*, *44*(11), 1797–1818. https://doi.org/10.1111/j.1945-5100.2009.tb01208.x

Eugster, O. (1988). Cosmic-ray production rates for $^{3}$He, $^{21}$Ne, $^{38}$Ar, $^{83}$Kr, and $^{126}$Xe in chondrites based on $^{81}$Kr-Kr exposure ages. *Geochim. Cosmochim. Acta*, *52*(6), 1649–1662. https://doi.org/10.1016/0016-7037(88)90233-5

Frick, U., and Pepin, R. O. (1981). Microanalysis of nitrogen isotope abundances: Association of nitrogen with noble gas carriers in Allende. *Earth Planet. Sci. Lett.*, *56*, 64–81. https://doi.org/10.1016/0012-821X(81)90117-5

Frick, U., Becher, R. H., and Pepin, R. O. (1988). Solar wind record in the lunar regolith—Nitrogen and noble gases. In *Proceedings of the 18th Lunar and Planetary Science Conference* (pp. 87–120). Houston, TX: Cambridge University Press.

Füri, E., and Marty, B. (2015). Nitrogen isotope variations in the Solar System. *Nat. Geosci.*, *8*(7), 515–522. https://doi.org/10.1038/NGEO2451

Gibson, E. K., Moore, C. B., and Lewis, C. F. (1971). Total nitrogen and carbon abundances in carbonaceous chondrites. *Geochim. Cosmochim. Acta*, *35*(6), 599–604. https://doi.org/10.1016/0016-7037(71)90089-5

Hashizume, K., Chaussidon, M., Marty, B., and Robert, F. (2000). Solar wind record on the moon: Deciphering presolar from planetary nitrogen. *Science*, *290*(5494), 1142–1145. https://doi.org/10.1126/science.290.5494.1142

Humbert, F., Libourel, G., France-Lanord, C., Zimmermann, L., and Marty, B. (2000). $CO_2$-laser extraction-static mass spectrometry analysis of ultra-low concentrations of nitrogen in silicates. *Geostand. Newslett.*, *24*(2), 255–260. https://doi.org/10.1111/j.1751-908X.2000.tb00777.x

Jiao, Y. F., Cheng, B., Huang, Y. K., Asphaug, E., Gladman, B., Malhotra, R., Michel, P., Yu, Y., and Baoyin, H. X. (2024). Asteroid Kamo'oalewa's journey from the lunar Giordano Bruno crater to Earth 1:1 resonance. *Nat. Astron.*, *8*(7), 819–826. https://doi.org/10.1038/s41550-024-02258-z

Kerridge, J. F. (1993). Long-term compositional variation in solar corpuscular radiation: Evidence from nitrogen isotopes in the lunar regolith. *Rev. Geophys.*, *31*(4), 423–437. https://doi.org/10.1029/93RG01953

Kung, C. C., and Clayton, R. N. (1978). Nitrogen abundances and isotopic compositions in stony meteorites. *Earth Planet. Sci. Lett.*, *38*(2), 421–435. https://doi.org/10.1016/0012-821X(78)90117-6

Lin, Y. T., Zhang, Y. H., Hu, S., Xu, Y. C., Zhou, W. J., Li, S. J., Yang, W., Gao, Y., Li, M. T., … Ip, W. (2020). Concepts of the small body sample return missions—The 1st 10 million year evolution of the solar system. *Space Sci. Rev.*, *216*(4), 45. https://doi.org/10.1007/s11214-020-00670-1

Liu, B., Liu, X. D., Jia, X. Y., Li, F., Zhao, Y. H., and Yu, L. L. (2023). Active asteroid 311P/PanSTARRS: Rotational instability as the origin of its multitails?. *Astron. J.*, *166*(4), 156. https://doi.org/10.3847/1538-3881/acf31c

Lodders, K. (2003). Solar system abundances and condensation temperatures of the elements. *Astrophys. J.*, *591*(2), 1220–1247. https://doi.org/10.1086/375492

Manuel, O. K., Wright, R. J., Miller, D. K., and Kuroda, P. K. (1972). Isotopic compositions of rare gases in the carbonaceous chondrites Mokoia and Allende. *Geochim. Cosmochim. Acta*, *36*(9), 961–983. https://doi.org/10.1016/0016-7037(72)90016-6

Mortimer, J., Verchovsky, A. B., Anand, M., Gilmour, I., and Pillinger, C. T. (2015). Simultaneous analysis of abundance and isotopic composition of nitrogen, carbon, and noble gases in lunar basalts: Insights into interior and surface processes on the Moon. *Icarus*, *255*, 3–17. https://doi.org/10.1016/j.icarus.2014.10.006

Okazaki, R., Marty, B., Busemann, H., Hashizume, K., Gilmour, J. D., Meshik, A., Yada, T., Kitajima, G., Broadley, M. W., … Tsuda, Y. (2022). Noble gases and nitrogen in samples of asteroid Ryugu record its volatile sources and recent surface evolution. *Science*, *379*(6634), eabo0431. https://doi.org/10.1126/science.abo0431

Reddy, V., Kuhn, O., Thirouin, A., Conrad, A., Malhotra, R., Sanchez, J. A., and Veillet, C. (2017). Ground-based Characterization of Earth Quasi Satellite (469219) 2016 $HO_3$. *AAS/Div. Planet. Sci. Meeting Abstr.*, *49*, 204.07.

Schultz, L., and Franke, L. (2004). Helium, neon, and argon in meteorites: A data collection. *Meteorit. Planet. Sci.*, *39*(11), 1889–1890. https://doi.org/10.1111/j.1945-5100.2004.tb00083.x

Thiemens, M. H., and Clayton, R. N. (1981). Nitrogen isotopes in the Allende meteorite. *Earth Planet. Sci. Lett.*, *55*(3), 363–369. https://doi.org/10.1016/0012-821X(81)90164-3

Wei, S. J., He, Y. Y., Liu, T. Y., Yang, W., and Lin, Y. T. (2024). History and implications of asteroid exploration. *Chin. J. Space Sci. (in Chinese)*, *44*(1), 19–50. https://doi.org/10.11728/cjss2024.01.2024-yg02

Wieler, R., Humbert, F., and Marty, B. (1999). Evidence for a predominantly non-solar origin of nitrogen in the lunar regolith revealed by single grain analyses. *Earth Planet. Sci. Lett.*, *167*(1-2), 47–60. https://doi.org/10.1016/S0012-821X(99)00012-6

Wieler, R. (2002). Noble gases in the solar system. *Rev. Mineral. Geochem.*, *47*(1), 21–70. https://doi.org/10.2138/rmg.2002.47.2

Wright, I. P., Boyd, S. R., Franchi, I. A., and Pillinger, C. T. (1988). High-precision determination of nitrogen stable isotope ratios at the sub-nanomole level. *J. Phys. E: Sci. Instrum.*, *21*(9), 865–875. https://doi.org/10.1088/0022-3735/21/9/011

Young, E. D., and Russell, S. S. (1998). Oxygen reservoirs in the early solar nebula inferred from an Allende CAI. *Science*, *282*(5388), 452–455. https://doi.org/10.1126/science.282.5388.452

Zhang, H., Cao, J. B., Lin, Y. T., Wei, Y., Li, L., Zhang, X. G., Lin, H. L., and Xie, L. H. (2023). Key questions of solar wind–Moon interaction. *Space Sci. Technol.*, *3*, 0060. https://doi.org/10.34133/space.0060

Zhang, X. H., Su, F., Avice, G., Stuart, F. M., Zheng, Y. Y., Liu, Z. H., Guo, W., Smith, T., Liu, R. C., … He, H. Y. (2024). Presence of non-solar derived krypton and xenon unveiled by Chang'e-5 lunar soils. *Earth Planet. Sci. Lett.*, *637*, 118725. https://doi.org/10.1016/j.epsl.2024.118725